Available online at www.sciencedirect.com
ScienceDirect
Trans. Nonferrous Met. Soc. China 32(2022) 1133−1143
Transactions of Nonferrous Metals Society of China
www.tnmsc.cn

Influence of chloride ion concentration on initial corrosion of AZ63 magnesium alloy

Branimir N. GRGUR[1], Branimir Z. JUGOVIĆ[2], Milica M. GVOZDENOVIĆ[1]

1. Faculty of Technology and Metallurgy, University of Belgrade, Karnegijeva 4, 11020 Belgrade, Serbia;
2. Serbian Academy of Science and Arts, Institute of Technical Science, Knez Mihailova 35, 11000 Belgrade, Serbia

Received 27 April 2021; accepted 9 December 2021

Abstract: The initial corrosion behavior of AZ63 magnesium alloy was investigated in 1, 3, 5 and 7 wt.% NaCl solutions by means of corrosion potential, linear polarization, electrochemical impedance spectroscopy, and polarization measurements, during exposure in the corrosion media. Results show that the increase in chloride concentration provokes an increase in the corrosion rate. Based on the obtained kinetics parameters the mechanisms of anodic dissolution and hydrogen evolution reactions were discussed, and kinetic models were proposed. It is concluded that anodic dissolution proceeds under Temkin conditions and hydrogen evolution reaction depends on the surface coverage of $Mg(OH)_2$ species.

Key words: chloride; corrosion potential; linear polarization; reaction order; kinetics

1 Introduction

Magnesium alloys due to their outstanding physicochemical properties, like low density, recyclability, biocompatibility, good corrosion resistance under specific conditions, excellent mechanical properties, etc., find applications in many different areas [1−3]. A broad range of applications include industrial applications as a construction material in automotive, aviation, and space technology [4,5], sacrificial anodes or additives to organic coatings in cathodic protection [6,7], primary and water-activated battery [8,9], biomedical applications [10−14], and hydrogen storage materials [15].

In the contact with dry air, a highly exothermic reaction of the Mg and Mg alloys occurred, forming the surface film with a few nanometers in thickness [16].

$$2Mg+O_2\rightarrow 2MgO\ \ (\Delta_rG^{\ominus}=-298.5\ \text{kJ/mol}) \quad (1)$$

Unfortunately, except indoor or some other environments, Mg and its alloy obey different kinds of corrosion, and form $Mg(OH)_2$, as suggested by many authors [4,6,16]. Nevertheless, in the contact with electrolyte if the corrosive medium contains chloride ions with the concentration beyond 150 mmol/L [17], the magnesium oxide/hydroxide will be converted to magnesium chloride ($MgCl_2$) that is highly soluble, 54.3 g/100 mL at 20 °C, in aqueous solution according to the following reaction [18]:

$$Mg(OH)_2+2Cl^-\rightarrow MgCl_2+2OH^- \quad (2)$$

Corrosion of Mg and its alloys was widely investigated [16], and the usual techniques for the investigation of the corrosion behavior, consist of immersion of the specimens in corrosive media, and measurement of evolved hydrogen and mass loss. Less attempt is given to classical electrochemical studies. For example, ZHAO et al [19] investigated the influence of pH and chloride ion concentration

Corresponding author: Branimir N. GRGUR, E-mail: BNGrgur@tmf.bg.ac.rs
DOI: 10.1016/S1003-6326(22)65861-8

on the corrosion of ZE41 Mg alloy using the immersion method and polarization measurements, in 0, 0.1, and 1 mol/L NaCl solutions with pH of 3, 7, and 11. They found that the hydrogen evolution rate is practically zero for immersion in the 0 mol/L NaCl solutions with pH 7 and 11. Besides, they observed that the hydrogen evolution rate increased with decreasing pH at each chloride ion concentration and with increasing chloride ion concentration at each pH. SHETTY et al [20] investigated the corrosion behavior of GA9 magnesium alloy in sulfate-containing solutions, 0.1 to 2 mol/L, and also observed that the corrosion potential is shifted to more negative values with the increase in sulfate ion concentration. In addition, they obtained high cathodic slopes in the range of −140 to −200 mV/dec. It should be accentuated that the negative differential effect (NDE) as an unusual electrochemical phenomenon that hydrogen evolution occurs under the anodic polarization, is widely observed in the corrosion of magnesium, its alloys, and some other metals [16,19,21]. Even few mechanisms are proposed to explain NDE, like the reaction of unipolar Mg^+ with water, formation, and decomposition of MgH_2, the most probable explanation is given by THOMAS et al [21], which suggests that when Mg is polarized anodically, the net dissolution current is a sum of two currents: (1) the electrochemical dissolution corresponding to the applied current for the reaction of $Mg \rightarrow Mg^{2+}+2e$ that can be recorded by the potentiostat; (2) the dissolution rate by the local corrosion reaction onto the surface of $Mg+2H_2O \rightarrow Mg(OH)_2+H_2$ that is undetectable to the potentiostat, and therefore does not correspond to the sum of currents available for the direct measurements.

ALTUN and SEN [22] investigated the influence of pH and chloride ion concentration for AZ63 alloy using immersion test method and found that corrosion rate decreased with increasing pH (pH=2, 3, 8, 11, and 11.5), and increased with the increase of the chloride ion concentration (from 0 to 2 mol/L). They also observed that in pH 3−10.5, the pH practically does not influence the corrosion rate in the solution with 0.01 and 0.2 mol/L of the chloride, while some small decrease in corrosion rate is observed in 0.6, 1, and 2 mol/L of chloride. Using the polarization measurements, they obtained similar results, with a much higher influence of chloride ion concentration on anodic branches than on cathodic branches of the polarization curve. Also, they proposed that the main corrosion product is $Mg(OH)_2$. ACHARYA and SHETTY [23] investigated the influence of chloride, sulfate in the range from 0.05 to 0.25 mol/L, and the temperature on the corrosion of AZ31 alloy. They concluded, using polarization and impedance measurements, that the concentration increase of both chloride and sulfate increases corrosion rate, but chloride being more aggressive. The temperature accelerates corrosion rate, obeying the Arrhenius type behavior. Using EDX and SEM after 3 h of immersion in corrosive media, they observed the formation of un-protective $Mg(OH)_2$ deposits. YANG et al [24] investigated corrosion of AZ63 alloy in natural seawater and 3.5 wt.% NaCl solution. They observed that AZ63 alloy corrodes faster in 3.5 wt.% NaCl solution than in seawater. After 24 h of immersion, the main surface species in seawater is found to contain $CaCO_3$ and $Mg(OH)_2$, while in 3.5 wt.% NaCl primarily $Mg(OH)_2$ and $Mg_2(OH)_3Cl{\cdot}4H_2O$. To investigate the AZ63 alloy in 3.5 wt.% NaCl using the polarization and electrochemical impedance spectroscopy, LI et al [25] obtained φ_{corr}=−1.587 V, J_{corr}=18.7 μA/cm^2, anodic and cathodic Tafel slopes of b_a=58 mV/dec and b_c=−134 mV/dec, respectively. From the impedance measurements, they observed the inductive loop, characteristics for Mg and Mg alloy [16], and determined the inductivity value (L) of 441 H·cm^2.

The corrosion of the magnesium alloy is time-dependent [26,27], so the aim of this work is to investigate the initial corrosion properties of the AZ63 magnesium alloy and the influence of chloride ion concentration, using different electrochemical techniques.

2 Experimental

As the electrode, the cast AZ63 magnesium alloy (EN-MAMgAl6Zn3), whose chemical composition is shown in Table 1, is obtained from the manufacturer Magal, Raška-Serbia, with dimensions of 2 cm×2 cm and thickness of 1 mm,

Table 1 Chemical composition of AZ63 alloy (wt.%)

Mg	Al	Zn	Fe	Si	Mn	Cu	Ni
91.12	5.95	2.54	0.0014	0.025	0.3	0.002	0.001

which was used as the working electrode after mechanical polishing with sandpaper, diamond paste and ultrasonic cleaning in acetone.

The electrolytes with 1, 3, 5 and 7 wt.% NaCl corresponding to 0.17, 0.51, 0.85 and 1.20 mol/L NaCl were used. All the experiments were conducted in a three-compartment glass cell with a volume of 150 cm^3, containing a separate compartment for the saturated calomel reference (SCE) and the platinum counter electrode. Electrochemical measurements are accompanied using the potentiostat-galvanostat Gamry 1010E. The measurements are a combination of recording the corrosion potentials with simultaneously performing linear polarization measurements, under φ_{corr} ±10 mV, during 3000 s, which is sufficient time for the stabilization of φ_{corr}, followed by the electrochemical impedance spectroscopy in the frequency range from 20 kHz to 0.2 Hz, and IR-corrected polarization measurements, at v=1 mV/s, starting from the established corrosion potentials ($\varphi_{corr,1}$), ~300 mV in cathodic direction, and backward scan in cathodic and anodic directions.

At the end of the anodic polarization measurements in 7 wt.% NaCl, the surface is cleaned by dipping for 1 min at room temperature in a solution containing 200 g/L chromium trioxide (CrO_3), 10 g/L of silver nitrate ($AgNO_3$), and 20 g/L of barium nitrate ($Ba(NO_3)_2$), followed by washing with distilled water and acetone. An optical microscope Olympus CX41 equipped with a digital camera and connected to the PC was used to analyze the samples.

3 Results

3.1 Corrosion potential, linear polarization and impedance

Figure 1(a) shows the dependence of the corrosion potentials for AZ63 alloy over time for different concentrations of NaCl. It can be seen that the corrosion potentials practically linearly decrease with increase in the concentration of NaCl from −1.55 V in 1 wt.% NaCl to −1.6 V in 7 wt.% NaCl (inset in Fig. 1(a)). This is in agreement with the report of CAIN et al [28] that increase of the Cl^- concentration provokes decrease of φ_{corr} for many Mg alloy compositions. This could be connected with the faster rate of AZ63 dissolution in higher NaCl concentrations, which is accompanied with

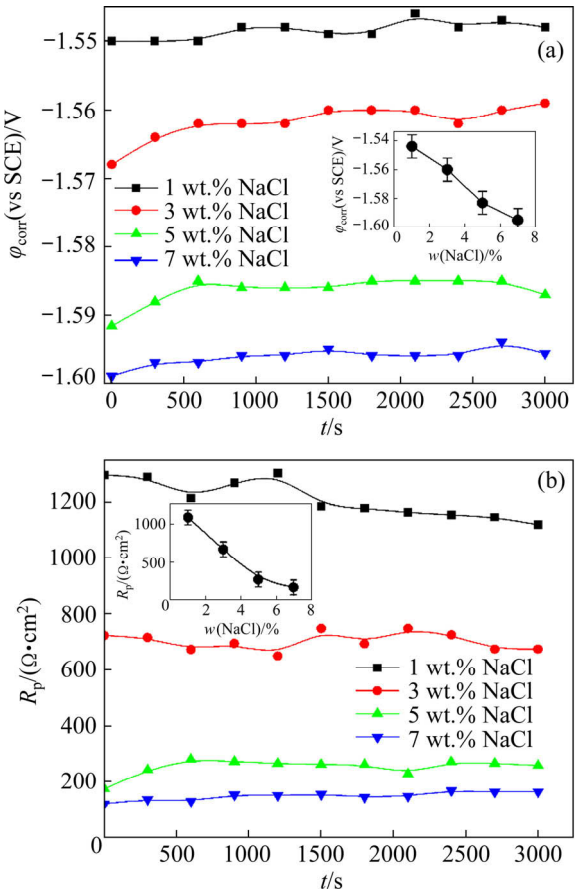

Fig. 1 Dependence of corrosion potential over time for different concentrations of NaCl (a) (Inset: The dependence of stable corrosion potential on NaCl concentrations), and dependence of polarization resistance over time for different NaCl concentrations (b) (Inset: The dependence of stable polarization resistance on NaCl concentrations)

the decrease of φ_{corr}. Over 3000 s, the corrosion potentials slightly change, for less than 5 mV, indicating that the surface reactions, like the formation of $Mg(OH)_2$ probably do not occur. Simultaneously with recording the corrosion potential, linear polarization measurements (±10 mV vs φ_{corr}) are performed, and results are shown in Fig. 1(b). It can be seen that, a very small variation of the polarization resistance (R_p), is observed over time in each NaCl solution, which additionally confirmed that the surface remains clean. The precipitation of low soluble salt will provoke an increase of R_p over time. The inset in Fig. 1(b) shows the values of R_p after 3000 s for different NaCl concentrations. R_p nonlinearly decreases with increasing NaCl concentration, indicating the fast corrosion reaction and the great

influence of chloride, because R_p is proportional to the reciprocal value of J_{corr}. For example, in 1 wt.% NaCl, polarization resistance is ~1100 Ω·cm^2, and in 7 wt.% NaCl, it is ~160 Ω·cm^2.

Figure 2 shows the Nyquist plots of the samples after 3000 s. All the impedance diagrams are characterized by one semicircle and low-frequency inductive loop. In the case of linear polarization measurements, the overall impedance increases with a decrease in NaCl concentration, indicating a decrease in the corrosion rate. The equivalent electrical circuits used for the fitting of experimental points, shown in Fig. 2, are adopted from KLOTZ [29]. In Fig. 2, R_0 represents the ohmic drop in the solution, and the double-layer capacitance is represented with constant phase elements (CPE_{dl}). The impedance of CPE is given as

$$Z = \frac{1}{Y_0(\mathrm{j}\omega)^n} \tag{3}$$

where n is related to the rotation angle of a purely capacitive line on the complex plane plots. For n=1, admittance Y_0=C_{dl}, $R_{p,1}$ and $R_{p,2}$ correspond to the corrosion processes, the resistance of cathodic and/or anodic reactions, while L is the inductivity, whose physical meaning is still under debate [30], but in general, can be associated with the process of the adsorption. From Fig. 2, it can be seen that fitted lines well correspond to the experimental points.

Determined parameters of the equivalent electrical circuits are shown in Fig. 3. The values of $R_{p,1}$ and $R_{p,2}$ practically linearly decrease with the increase in NaCl concentration. According to KING et al [31], polarization resistance, as a frequency-independent part, from the impedance measurements can be given as

$$\frac{1}{R_{p,imp}} = \frac{1}{R_{p,1}} + \frac{1}{R_{p,2}} \tag{4}$$

The calculated value of $R_{p,imp}$ is in good agreement with that obtained by the linear polarization measurements, $R_{p,lp}$, which is also shown in Fig. 3 for the comparison. Inset in Fig. 3 shows the determined values of admittance and inductivity. Because the parameter n in Eq. (3) is in all cases higher than 0.95, the admittance can be considered as capacitance. Therefore, the double-layer capacitance slightly decreases from 17.5 to 15 μF/cm^2 with the increase of the NaCl concentration. Such value indicates the existence of pure metallic surfaces, without semiconducting or insulating deposits. The value of the inductivity decreases practically linearly from 570 to ~40 H·cm^2, and as mentioned by KLOTZ [29], the inductivity can easily reach values much higher than 100 H·cm^2, but there is no physical explanation for such a high value.

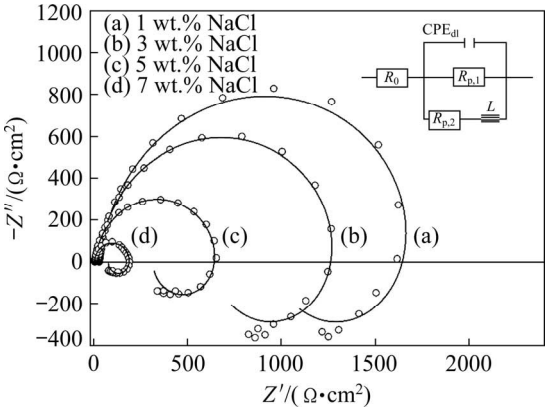

Fig. 2 Nyquist plots of samples after 3000 s for different concentrations of NaCl (Inset is the equivalent electrical circuits used for the fitting of experimental points)

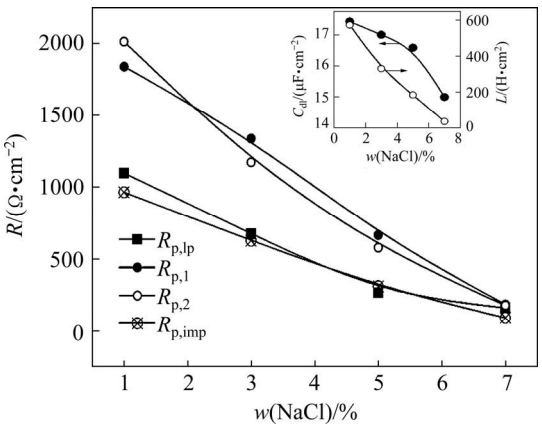

Fig. 3 Determined resistivity parameters of equivalent electrical circuits for different NaCl concentrations (Inset shows determined capacitance and inductivity for different NaCl concentrations)

3.2 Polarization curve

The typical *IR*-drop corrected polarization curve for the AZ63 alloy in 7 wt.% NaCl solution is shown in Fig. 4. The curve is recorded after impedance measurements, starting from established corrosion potential ($\varphi_{corr,1}$) in cathodic direction (forward scan) and reversing to ~200 mV that is more positive than $\varphi_{corr,1}$ (backward scan). In the

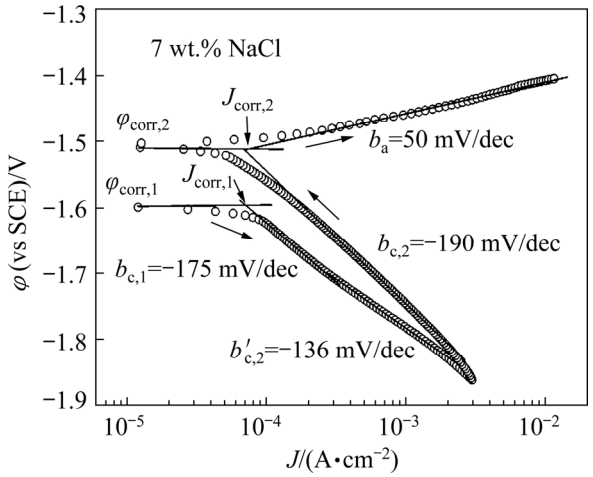

Fig. 4 *IR*-drop corrected polarization curve of AZ63 alloy in 7 wt.% NaCl solution

forward scan, some unusual behavior is observed. First, the slope of the cathodic curve has a high value of −175 mV/dec, and at the increased current density it changed to a smaller value of −135 mV/dec. Extrapolating the first slope to $\varphi_{corr,1}$, the corrosion current density of 71 μA/cm^2 is estimated. In the backward scan, the slope is again very high with the value of −190 mV/dec. Such strange behavior, which cannot be explained by the formal kinetics, suggests some parallel processes during cathodic polarization. At the potential for $\varphi_{corr,2}$ of 100 mV that is more positive than $\varphi_{corr,1}$, typical Tafel anodic behavior of active metal dissolution with the slope of b_a=50 mV/dec occurred. Extrapolating anodic Tafel slope to $\varphi_{corr,2}$, the $J_{corr,2}$ of 75 μA/cm^2 is obtained. A similar anodic slope of 60−80 mV/dec and cathodic slope of −150 to −220 mV/dec are obtained by MENA-MORCILLO and VELEVA [32] in the Ringer's, Hanks', and simulated body fluid solutions.

Comparable results (Fig. 5) are obtained in the solution with different chloride ions concentrations. It is characteristic that both $\varphi_{corr,1}$ and $\varphi_{corr,2}$ decrease with increase in NaCl concentration. Also, the forward and backward cathodic slopes have unusually high values greater than −150 mV/dec, with more or less pronounced second $b'_{c,2}$ slope, lower forward slope, b'_c, while the anodic single Tafel slopes slightly decreased from 57 to 50 mV/dec. In all cases, the increase in chloride concentrations provokes high corrosion current densities and high cathodic and anodic activities. It should be also mentioned that the anodic branches of the polarization curve are more affected by the change in NaCl concentration than cathodic ones. The summarized kinetic parameters obtained from Fig. 5 are shown in Table 2 and Fig. 6.

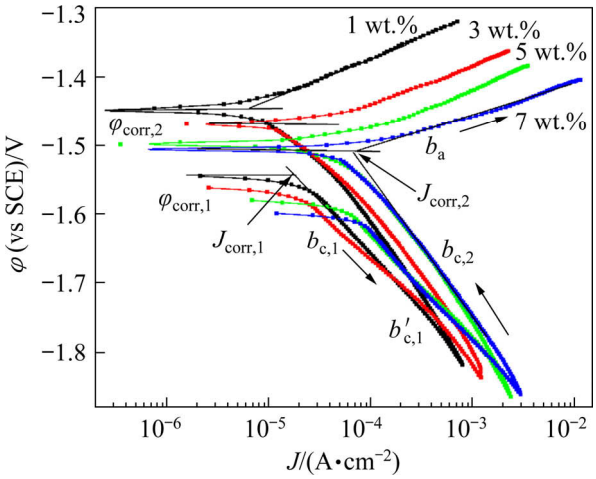

Fig. 5 *IR*-drop corrected polarization curves in solutions with different NaCl concentrations

In Fig. 6, the determined corrosion parameters are graphically presented. Corrosion current density increases with the increase of NaCl concentration. Except for 1 wt.% NaCl, $J_{corr,1}$ and $J_{corr,2}$ are practically the same. Corrosion potentials decrease with the increase in NaCl concentrations (Fig. 6(a), approximately 50 mV). Interestingly, the differences of $\varphi_{corr,1}$ and $\varphi_{corr,2}$ in all investigated solutions are practically the same, ~100 mV, for

Table 2 Determined kinetics parameters from polarization measurement for AZ63 alloy with different NaCl concentrations in solution

w(NaCl)/%	$\varphi_{corr,1}$(vs SCE)/V	$b_{c,1}$/(mV·dec^{-1})	$b_{c,2}$/(mV·dec^{-1})	$J_{corr,1}$/(μA·cm^{-2})	$\varphi_{corr,2}$(vs SCE)/V	b_a/(mV·dec^{-1})	$J_{corr,2}$/(μA·cm^{-2})
1	−1.545	−159	−180	16	−1.449	57	6.3
3	−1.562	−157	−158	21	−1.4691	56	30
5	−1.589	−157	−175	50	−1.501	55	46
7	−1.599	−175	−190	71	−1.508	50	75

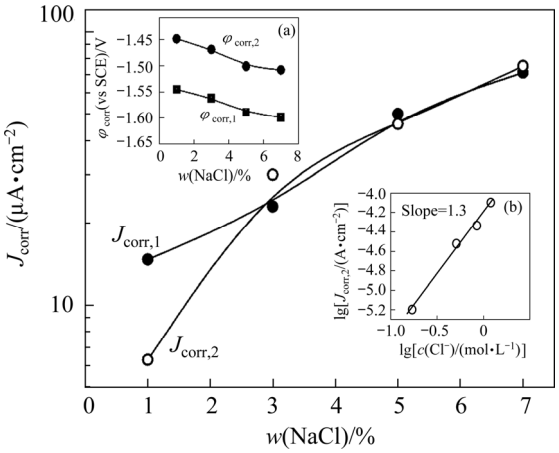

Fig. 6 Dependence of corrosion current densities $J_{corr,1}$, $J_{corr,2}$ on NaCl concentration (Insets: (a) Dependence of corrosion potential on NaCl concentration; (b) Dependence of logarithm of $J_{corr,2}$ over mole concentration of Cl^-)

which we do not have a reasonable explanation. To determine reaction order in respect to chloride the following analysis is performed. Because anodic curves show much more reliable dependence than cathodic ones, the reaction order is estimated from $J_{corr,2}$. The partial anodic current for the corrosion process can be given as

$$J = zFk_a c^p(Cl^-)\exp\left[\frac{2.3(\varphi-\varphi_{corr,2})}{b_a}\right] = \\ = J_{corr,2}\exp\left[\frac{2.3(\varphi-\varphi_{corr,2})}{b_a}\right] \quad (5)$$

where z is the number of exchanged electrons, F is the Faraday constant, k_a is the rate constant, φ is the actual electrode potential, and p is the reaction order with respect to Cl^- ion. In the case when actual electrode potential, φ, is equal to the corrosion potential, $\varphi_{corr,2}$, Eq. (5) becomes $J=J_{corr,2}$.

Extending this equation, the following is obtained:

$$J_{corr,2} = zFk_a c^p(Cl^-) \quad (6)$$

or after presenting Eq. (6) as a logarithm:

$$\lg J_{corr,2} = \lg(zFk_a) + p\lg c(Cl^-) \quad (7)$$

Consequently, from the slope of $\lg J_{corr,2}$ vs $\lg c(Cl^-)$, the partial reaction order of p=1.3 is determined (Fig. 6(b)). Also, under the conditions of $c(Cl^-)$=1 mol/L, $\lg J_{corr,2}=\lg(zFk_a)$, so $J_{corr,2}=60\times10^{-6}$ A/cm^2, $k_a=3.1\times10^{-10}$ mol/(s·cm^2) are estimated.

3.3 Optical micrograph

The optical image of the freshly polished surface of AZ63 alloy is shown in Fig. 7(a). The microstructure of the alloy consists of a randomly distributed β-phase ($Mg_{17}Al_{12}$) in the main body of the α-phase. Some dark spots could be assigned to the Al_8Mn_5 phase, as observed by WU et al [33] using EDS and SEM techniques. After the anodic polarization curve in 7 wt.% NaCl (Fig. 7(b)), it is obvious that corrosion occurs along the grain of α-phase. Corrosion product is probably connected with more noble phases like β-phase, Al_8Mn_5 phase, and Al, Zn, and other metallic impurities. It can be seen from Fig. 7(b) that the corrosion product is much darker than the rest of the surfaces and could be connected to the "dark regions" observed by many researchers during the Mg and Mg alloys corrosion [21,34]. This dark region contains an iron impurity that could be responsible for the negative differential effect.

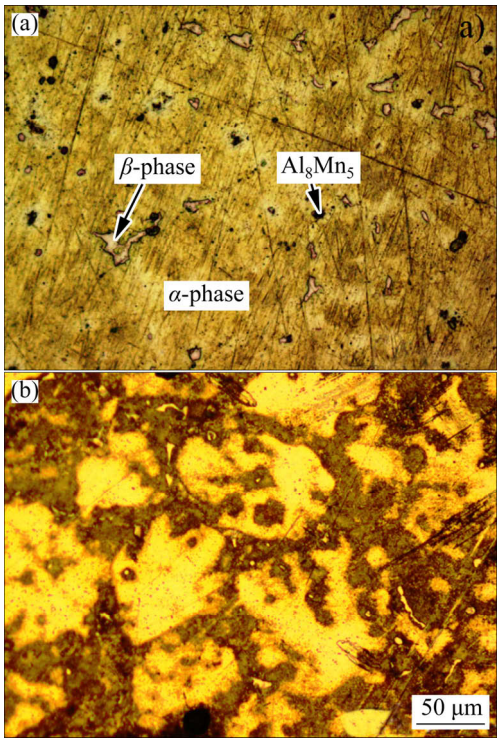

Fig. 7 Optical micrographs of AZ63 alloy: (a) Freshly polished surface; (b) After anodic polarization in 7 wt.% NaCl solution

4 Discussion

4.1 Thermodynamic calculation

One of the most important matters for the explanation of the corrosion behavior is the state of

AZ63 surface at the corrosion potential. Due to the low solubility product, K_{sp}, of ~1.1×10^{-11} mol^3/L^3, the precipitation of $Mg(OH)_2$ onto the electrode will occur only above some critical pH which can be calculated using the following equation:

$$pH_{crit} = -\lg a(H^+) = -\lg\left(K_w \Big/ \sqrt{\frac{K_{sp}}{c(Mg^{2+})}} \right) \quad (8)$$

where K_w is the ionic product of water 1×10^{-14} mol^2/L^2, and $c(Mg^{2+})$ is the actual concentration of the magnesium ions in the solution. The concentration of Mg^{2+} can be estimated from the open circuit measurements and using corrosion current density, $J_{corr,1}$ (Table 2), obtained from the polarization measurements:

$$c(Mg^{2+}) = \frac{n(Mg^{2+})}{V} = \frac{J_{corr,1}At}{2VF} \quad (9)$$

where A (cm^2) is the electrode surface area, and V (dm^3) is the electrolyte volume. The calculated concentrations after 3000 s of exposure to the $\varphi_{corr,1}$ are shown in the inset in Fig. 8, ranging from 10 to 65 μmol/L. With these values, using Eq. (8), pH_{crit} is calculated and shown in Fig. 8, and it decreases from ~11 for 1 wt.% NaCl to 10.6 for 7 wt.% NaCl.

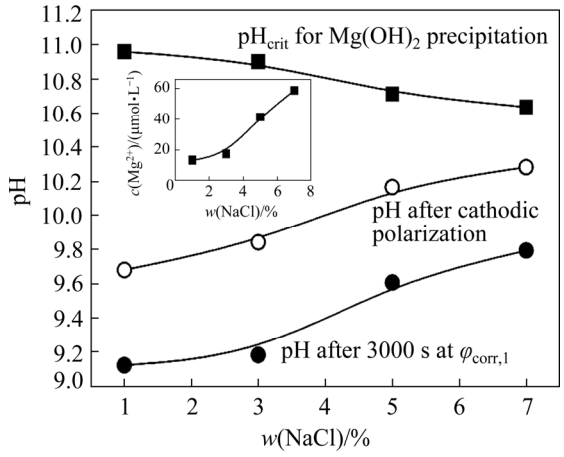

Fig. 8 Calculated values of pH over NaCl concentration after electrode being exposed for 3000 s at $\varphi_{corr,1}$, after cathodic polarization from $\varphi_{corr,1}$ to $\varphi_{corr,2}$, and critical pH for $Mg(OH)_2$ precipitation (Inset shows Mg^{2+} concentration formed during 3000 s of immersion, Eq. (9))

During the Mg corrosion, the concentration of OH^- also increases, due to the evolution of the hydrogen at the corrosion potential, and pH can be calculated using the following equation:

$$pH = -\lg a(H^+) = -\lg \frac{K_w}{c_0(OH^-) + \Delta c(OH^-)} \quad (10)$$

where $\Delta c(OH^-)$ can be calculated using the following equation:

$$\Delta c(OH^-) = \frac{n(OH^-)}{V} = \frac{J_{corr,1}At}{2VF} \quad (11)$$

For the initial pH of 6.8, the concentration of OH^- is $c_0(OH^-)=5\times10^{-8}$ mol/L, and after 3000 s at $\varphi_{corr,1}$ pH increases from 9.1 for 1 wt.% NaCl to 9.8 for 7 wt.% NaCl and that is insufficient for the precipitation of $Mg(OH)_2$. This can explain the constant value of $\varphi_{corr,1}$ (Fig. 1(a)) and R_p during 3000 s (Fig. 1(b)). If the precipitation of $Mg(OH)_2$ occurs, R_p will increase over time. Also, if we in the first approximation neglect near electrode pH, stabilized pH of the solution after cathodic polarization can be calculated from Eq. (12):

$$\Delta c_{cat}(OH^-) = \frac{n(OH^-)}{V} = \frac{A\int J_c dt}{2VF} \quad (12)$$

where the integral is the total area for the forward and backward cathodic scan (I vs t graph, not shown) for each curve between $\varphi_{corr,1}$ and $\varphi_{corr,2}$ (Fig. 5). So the final solution pH can be calculated by

$$pH_{cat} = -\lg \frac{K_w}{c_0(OH^-) + \Delta c(OH^-) + \Delta c_{cat}(OH^-)} \quad (13)$$

The calculated values for the solution pH after cathodic polarization range from 9.7 to 10.3 (Fig. 8). So, even during the cathodic polarization near electrode pH could be higher than pH_{crit}, the eventually formed $Mg(OH)_2$ will be dissolved with the assistance of chloride anions after pH equalizes near the electrode and the bulk of the solution. YANG et al [24] investigated the evolution of the corrosion morphology under natural seawater immersion using SEM. For 2 h of immersion, the surface of the alloy remains practically unaffected. Pits and development of the surface deposits can be seen after immersion for 6 and 12 h, and for 24 h, the surface of AZ63 alloy is nearly entirely covered by the regular and compact deposits. It should be mentioned that near-surface pH during potential step experiments on gold in unbuffered pH 4, 0.33 mol/L Na_2SO_4 solution for different applied electrode potentials, even reached pH~11 within 60 s at –1.1 V (vs Ag/AgCl), for the very fast time ~120 s is equalized to its initial value [35]. In

principle, from these calculations, it can be concluded that AZ63 alloy at the corrosion potential after 3000 s of immersion and cathodic polarization is in the practically metallic state, or slightly covered with film-forming deposits at the most active cathodic sites.

Hence, based on the presented thermodynamic calculations, it could be postulated that AZ63 alloy after being exposed for ~1 h to different concentrations of NaCl, is in its metallic state onto the surface.

4.2 Kinetics of AZ63 alloy anodic dissolution

The kinetic of AZ63 alloy is strongly influenced by the chloride concentration. Anodic dissolution of AZ63 alloy can be explained based on the determined kinetic parameters, by the following mechanisms,

$$\mathrm{Mg+Cl^-} \underset{k_{-1}}{\overset{k_1}{\rightleftharpoons}} \mathrm{Mg-Cl_{ads}+e} \quad (14)$$

$$\mathrm{Mg-Cl_{ads}+Cl^-} \xrightarrow{k_2} \mathrm{Mg^{2+}+2Cl^-+e\ \ (r.d.s)} \quad (15)$$

with the rate-determining step (r.d.s) given by Eq. (15). The existence of the adsorbed chloride species can explain the inductive loop observed in the electrochemical impedance measurements. Considering the Tafel slope of ~60 mV/dec and fractional reaction order in respect to chloride of 1.3, it could be proposed that lateral interaction of the adsorbed species onto the surface existed, so Temkin adsorption isotherm should be considered. The partial current density for the rate-determining step can be given as

$$J = k_2 F\theta c(\mathrm{Cl^-}) \exp\left(\frac{\gamma r\theta}{RT}\right) \exp\left(\frac{\alpha F\varphi}{RT}\right) \quad (16)$$

where θ is the surface coverage with adsorbed intermediates, γ and α are the symmetry of the activation barriers (in most cases for the elementary step γ and α are equal to 0.5), r is the interaction parameter for the Temkin adsorption isotherm. For the quasi-equilibrium of Eq. (14), Eq. (16) can be written as

$$k_1 F(1-\theta) c(\mathrm{Cl^-}) \exp\left(-\frac{\gamma r\theta}{RT}\right) \exp\left(\frac{\alpha F\varphi}{RT}\right) = k_{-1} F\theta \exp\left(\frac{\gamma r\theta}{RT}\right) \exp\left(-\frac{\alpha F\varphi}{RT}\right) \quad (17)$$

Because pre-exponential term containing θ is changing much less than exponential term, it could be considered as constant, and taking into account that γ=α=0.5, it can be written as

$$k_1' c(\mathrm{Cl^-}) \exp\left(-\frac{r\theta}{2RT}\right) \exp\left(\frac{F\varphi}{2RT}\right) = k_{-1}' \exp\left(\frac{r\theta}{2RT}\right) \exp\left(-\frac{F\varphi}{2RT}\right) \quad (18)$$

After rearrangement, Eq. (18) can be written as

$$\exp\left(\frac{r\theta}{RT}\right) = \frac{k_1'}{k_{-1}'} c(\mathrm{Cl^-}) \exp\left(\frac{F\varphi}{RT}\right) \quad (19)$$

After taking the square root,

$$\exp\left(\frac{r\theta}{2RT}\right) = \left(\frac{k_1'}{k_{-1}'}\right)^{0.5} c^{0.5}(\mathrm{Cl^-}) \exp\left(\frac{F\varphi}{2RT}\right) \quad (20)$$

Finally, after introducing Eq. (20) into the equation of the rate-determining step, Eq. (16), one can obtain

$$J = Kc^{3/2}(\mathrm{Cl^-}) \exp\left(\frac{F\varphi}{RT}\right) \quad (21)$$

Theoretically, the anodic Tafel slope will have the value of 60 mV/dec, 2.3RT/F, and reaction order with respect to chloride 1.5, which is very near to the experimentally determined values.

4.3 Kinetics of hydrogen evolution reaction

Unusual behavior during the hydrogen evolution reaction could be explained as follows. Assuming the classical Volmer-Heyrovsky mechanism,

$$\mathrm{H_2O+e} \xrightarrow{k_{1,V}} \mathrm{H_{ads}+OH^-\ (r.d.s)} \quad (22)$$

$$\mathrm{H_{ads}+H_2O+e} \underset{k_{-2H}}{\overset{k_{2H}}{\rightleftharpoons}} \mathrm{H_2+OH^-} \quad (23)$$

with rate determining Volmer step, the cathodic current under Langmuir conditions can be given as

$$j = k_1 F(1-\theta_{\mathrm{H}}) \exp\left(-\frac{\alpha F\varphi}{RT}\right) \quad (24)$$

which predicts the Tafel slope of −120 mV/dec and zero reaction order with respect to hydrogen ions when $\theta_{\mathrm{H}} \to 0$, and $k_{1,\mathrm{V}} \ll k_{2,\mathrm{H}}$, which is observed by ALTUN and SEN [22]. But, considering that during cathodic polarization $2\mathrm{OH^-}$ is released, the pH near the electrode can increase above critical pH, and $\mathrm{Mg(OH)_2}$ can precipitate onto the electrode because $\mathrm{Mg^{2+}}$ ions are present in the solution. Therefore, the cathodic current should include one more term, e.g. $[1-\theta(\mathrm{Mg(OH)_2})]$, so Eq. (24) becomes

$$J = k_1 F[1-\theta(\mathrm{Mg(OH)_2})]\exp\left(-\frac{\alpha F\varphi}{RT}\right) \quad (25)$$

or for a real case of cathodic evolution of hydrogen on AZ63 alloy.

$$J = J_{\mathrm{corr},1}[1-\theta(\mathrm{Mg(OH)_2})]\exp\left(-\frac{2.3(\varphi-\varphi_{\mathrm{corr},1})}{|b_c|}\right) \quad (26)$$

The formal kinetics usually neglects the influence of the pre-exponential term. By the influence of the pre-exponential term, the Tafel slope is a function of $\partial[1-\theta]/\partial\varphi$. Consequently, when this term increases the Tafel slope also increases, when it is a constant over some potentials range the Tafel slope will be −120 mV/dec. This can be clearly seen in Fig. 9(a), where the simulation of Eq. (26) is shown, using the experimentally determined values for $\varphi_{\mathrm{corr},1}$ and $J_{\mathrm{corr},1}$ in 7 wt.% NaCl. In the first case, the $\theta[\mathrm{Mg(OH)_2}]$ is small and constant (inset in Fig. 9(a)), over the entire potential range, and the Tafel slope is −120 mV/dec. In the second case, $\theta[\mathrm{Mg(OH)_2}]$ linearly increases from ~0 to 0.8, and the Tafel slope is −160 mV/dec. Unusual cathodic curves with hysteresis for hydrogen evolution reaction in 7 wt.% NaCl (Fig. 4), could be explained in a similar way. Taking the experimentally determined values of $\varphi_{\mathrm{corr},1}$ and $J_{\mathrm{corr},1}$ and $\varphi_{\mathrm{corr},2}$ and $J_{\mathrm{corr},2}$ (Table 2), the polarization curves are simulated by Eq. (26), for the nonlinear change of $\theta[\mathrm{Mg(OH)_2}]$ (inset of Fig. 9(b)). In the forward scan $\theta[\mathrm{Mg(OH)_2}]$ linearly changes from $\varphi_{\mathrm{corr},1}$ up to the potential of −1.7 V, and after that due to the decrease of Mg^{2+} concentration near the electrode, changes are much smaller. As a consequence, the Tafel slope in the region of low current densities has a high value of −176 mV/dec, followed by a smaller Tafel slope of −136 mV/dec, in the higher current density range (Fig. 9(b)). In the backward scan, the decrease in term $\theta[\mathrm{Mg(OH)_2}]$ is slightly changed due to the kinetics of the reaction of $Mg(OH)_2+2Cl^-=MgCl_2+2OH^-$, and due to the release of additional OH^- ions the $\theta[\mathrm{Mg(OH)_2}]$ could be with small value present on the electrode surface up to the $\varphi_{\mathrm{corr},2}$. So, such a change of $\theta[\mathrm{Mg(OH)_2}]$ gives a polarization curve with a slope of −185 mV/dec. Therefore, the change of the surface coverage of $1-\theta[\mathrm{Mg(OH)_2}]$ part can give the Tafel slop from −120 mV/dec up to the infinity for the conditions when $\theta[\mathrm{Mg(OH)_2}]\rightarrow 1$.

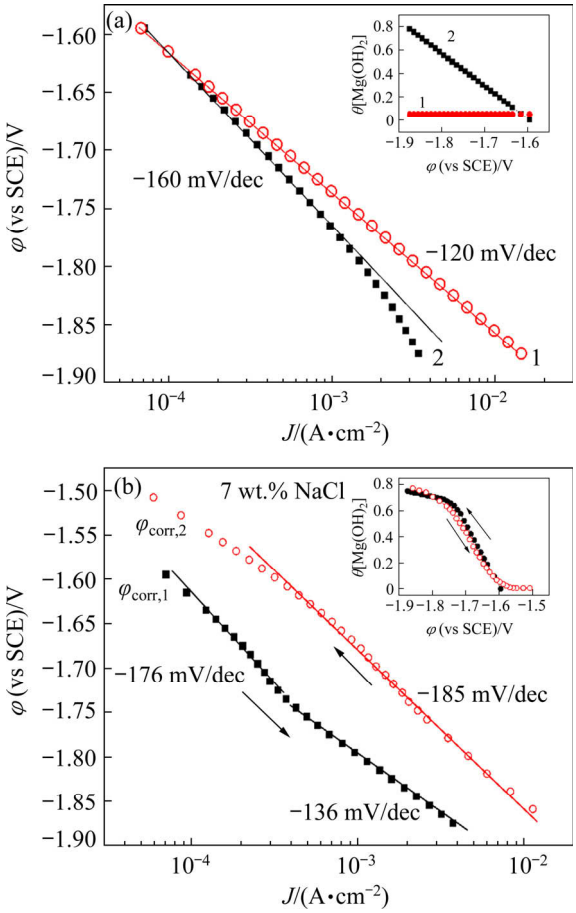

Fig. 9 Simulation of Eq. (26) with $\varphi_{\mathrm{corr},1}$ and $J_{\mathrm{corr},1}$ in 7 wt.% NaCl and different $\theta[\mathrm{Mg(OH)_2}]$ (a), and with $\varphi_{\mathrm{corr},1}$ and $J_{\mathrm{corr},1}$ for forward, and with $\varphi_{\mathrm{corr},2}$ and $J_{\mathrm{corr},2}$ for backward scan in 7 wt.% NaCl and different $\theta[\mathrm{Mg(OH)_2}]$ (b)

The proposed mechanism cannot explain higher activity for the hydrogen evolution reaction with increase in chloride concentration (Fig. 5). This can be explained by the sporadic formation of dark regions at corrosion potentials, which contained iron impurities [34]. Increasing the chloride concentration, more dark regions are formed by the anodic metal dissolution, and exchange current density for hydrogen evolution reaction varies for different chloride concentrations, provoking the higher corrosion current density and higher activity for hydrogen evolution reaction. One more issue should be explained. Namely, from Fig. 6(a), it can be seen that $\varphi_{\mathrm{corr},2}$ is more positive than $\varphi_{\mathrm{corr},1}$. This can be explained by the kinetics of magnesium oxy/hydroxide dissolution (Reaction (2)). At $\varphi_{\mathrm{corr},1}$, $\theta[\mathrm{Mg(OH)_2}]$ is rather small, and by the forward cathodic polarization, more $Mg(OH)_2$ is formed onto the surface by the film-forming

mechanism. In the backward cathodic polarization, $Mg(OH)_2$ is slowly dissolved due to pH near electrode equalization below pH_{crit}, the influence of the chloride anions, and $\theta[Mg(OH)_2]$ becomes ~0 at more positive potentials. This can also explain why the corrosion potential is more negative in the solutions with higher concentrations of chloride anions. Eventually formed $Mg(OH)_2$ is faster dissolving in the presence of higher concentrations of the chloride anions, provoking a decrease in corrosion potentials.

5 Conclusions

(1) Based on the measurements of the open-circuit potentials, linear polarization, electrochemical impedance spectroscopy, and the thermodynamic considerations, during the initial period of immersion, ~3000 s, in different NaCl concentrations, AZ63 Mg alloy indicates that the surface reactions, like the formation of $Mg(OH)_2$ probably do not occur.

(2) The corrosion potentials linearly decrease with increase in the concentration of chloride from –1.55 V in 1 wt.% NaCl to −1.6 V in 7 wt.% NaCl.

(3) The corrosion current density increases with the increase of chloride concentration in the range of 16 to 70 μA/cm^2.

(4) From the polarization curves, the anodic Tafel slope in the range of ~60 mV/dec, fractional reaction order in respect to the chloride of 1.3, and high cathodic slopes of −130 to −190 mV/dec, are determined.

(5) Based on the obtained kinetics parameters, it is suggested that anodic dissolution obeys the Temkin adsorption isotherm, and the cathodic reaction is dictated by the increase of magnesium oxy/hydroxide coverage onto the electrode surfaces.

Acknowledgments

This work is supported by the Ministry of Education, Science and Technological Development of the Republic of Serbia (Nos. 451-03-9/2021-14/200135, 451-03-9/2021-14/200175)

References

[1] LUO A A. Magnesium casting technology for structural applications [J]. Journal of Magnesium and Alloys, 2013, 1: 2−22.

[2] SONG J F, SHE J, CHEN D L, PAN F S. Latest research advances on magnesium and magnesium alloys worldwide [J]. Journal of Magnesium and Alloys, 2020, 8: 1−41.

[3] KHOKHLOVA J, KHOKHLOV M, SYNYUK V. Magnesium alloy AZ63A reinforcement by alloying with gallium and using high-disperse ZrO_2 particles [J]. Journal of Magnesium and Alloys, 2016, 4(4): 265−269.

[4] SONG G L, ATRENS A. Corrosion mechanisms of magnesium alloys [J]. Advanced Engineering Materials, 1999, 1: 11−33.

[5] YUAN Ding-ling, CHEN Song-yi, CHEN Kang-hua, HUANG Lan-ping, CHANG Jiang-yu, ZHOU Liang, DING Yun-feng. Correlations among stress corrosion cracking, grain-boundary microchemistry, and Zn content in high Zn-containing Al−Zn−Mg−Cu alloys [J] Transactions of Nonferrous Metals Society of China, 2021, 31(8): 2220−2231.

[6] PATHAK S S, MENDON S K, BLANTON M D, RAWLINS J W. Magnesium-based sacrificial anode cathodic protection coatings (Mg-rich primers) for aluminum alloys [J]. Metals, 2012, 2(3): 353−376.

[7] KIM J G, KIM Y W. Advanced Mg−Mn−Ca sacrificial anode materials for cathodic protection [J]. Materials and Corrosion, 2001, 52: 137−139.

[8] VUORILEHTO K, RAJANTIE H. Water-activated cuprous bromide battery [J]. Journal of Applied Electrochemistry, 1999, 29: 903−911.

[9] SONG Yan, YANG Hua-bao, CHAI Yan-fu, WANG Qing-hang, JIANG Bin, WU Liang, ZOU Qin, HUANG Guang-sheng, PAN Fu-sheng, ATRENS A. Corrosion and discharge behavior of Mg−xLa alloys (x=0.0−0.8) as anode materials [J]. Transactions of Nonferrous Metals Society of China, 2021, 31(7): 1979−1992.

[10] BOMMALA V K, KRISHNA M G, RAO C T. Magnesium matrix composites for biomedical applications: A review [J]. Journal of Magnesium and Alloys, 2019, 7: 72−79.

[11] PERON M, TORGERSEN J, BERTO F. Mg and its alloys for biomedical applications: Exploring corrosion and its interplay with mechanical failure [J]. Metals, 2017, 7(7): 252.

[12] LUDGER K L, WEBER L, van HUMBEECK J, MORTENSEN A, LUYTEN J, SCHROOTEN J. Open cellular magnesium alloys for biodegradable orthopaedic implants [J]. Journal of Magnesium and Alloys, 2013, 1(4): 303−311.

[13] WANG Xue-jian, CHEN Zong-ning, ZHANG Yu-bo, GUO En-yu, KANG Hui-jun, HAN Pei, WANG Tong-min, Influence of microstructural characteristics on corrosion behavior of Mg−5Sn−3In alloy in Hank's solution [J] Transactions of Nonferrous Metals Society of China, 2021, 31(10): 2999−3011.

[14] MA Ying-zhong, WANG De-xin, LI Hong-xiang, YANG Chang-lin, YUAN Fu-song, ZHANG Ji-shan. Microstructure, mechanical properties and corrosion behavior of quaternary Mg−1Zn−0.2Ca−xAg alloy wires applied as degradable anastomotic nails [J] Transactions of Nonferrous Metals Society of China, 2021, 31(1): 111−124.

[15] LUO Q, LI J D, LI B, LIU B, SHAO H Y, LI Q. Kinetics in Mg-based hydrogen storage materials: Enhancement and mechanism [J]. Journal of Magnesium and Alloys, 2019, 7:

58−71.
[16] ESMAILY M, SVENSSON J E, FAJARDO S, BIRBILIS N, FRANKEL G S, VIRTANEN S, ARRABAL R, THOMAS S, JOHANSSON L G. Fundamentals and advances in magnesium alloy corrosion [J]. Progress in Materials Science, 2017, 89: 92−193.
[17] SHAW B A. Corrosion resistance of magnesium alloys [M]// ASM Handbook. Metals Park, OH, USA: ASM International Handbook Committee, 2003.
[18] STAIGER M P, PIETAK A M, HUADMAI J, DIAS G. Magnesium and its alloys as orthopedic biomaterials: A review [J]. Biomaterials, 2006, 27: 1728−1734.
[19] ZHAO Ming-chun, LIU Ming, SONG Guang-ling, ATRENS A. Influence of pH and chloride ion concentration on the corrosion of Mg alloy ZE41 [J]. Corrosion Science, 2008, 50: 3168−3178.
[20] SHETTY S, NAYAK J, SHETTY A N. Influence of sulfate ion concentration and pH on the corrosion of Mg−Al−Zn−Mn (GA9) magnesium alloy [J]. Journal of Magnesium and Alloys, 2015, 3: 258−270.
[21] THOMAS S, MEDHEKAR N V, FRANKEL G S, BIRBILIS N. Corrosion mechanism and hydrogen evolution on Mg [J]. Current Opinion in Solid State and Materials Science, 2015, 19: 85−94.
[22] ALTUN H, SEN S. Studies on the influence of chloride ion concentration and pH on the corrosion and electrochemical behaviour of AZ63 magnesium alloy [J]. Materials & Design, 2004, 25: 637−643.
[23] ACHARYA M G, SHETTY A N. The corrosion behavior of AZ31 alloy in chloride and sulfate media—A comparative study through electrochemical investigations [J]. Journal of Magnesium and Alloys, 2019, 7: 98−112.
[24] YANG L H, LIN C G, GAO H P, XU W C, LI Y T, HOU B R, HUANG Y L. Corrosion behaviour of AZ63 magnesium alloy in natural seawater and 3.5 wt.% NaCl aqueous solution [J]. International Journal of Electrochemical Science, 2018, 13: 8084−8093.
[25] LI J R, WAN K, JIANG Q T, SUN H Y, LI Y T, HOU B R, ZHU L W, LIU M. Corrosion and discharge behaviors of Mg−Al−Zn and Mg−Al−Zn−In alloys as anode materials [J]. Metals, 2016, 6(3): 65.
[26] PINELA V M, de OLIVEIRA L A, de OLIVEIRA M C L, ANTUNES R A. Study of the corrosion process of AZ91D magnesium alloy during the first hours of immersion in 3.5 wt.% NaCl solution [J]. International Journal of Corrosion, 2018, 2018: 8785154.
[27] ATRENS A, SONG G L, CAO F Y, SHI Z M, BOWEN P K. Advances in Mg corrosion and research suggestions [J]. Journal of Magnesium and Alloys, 2013, 1: 177−200.
[28] CAIN T, BLAND L G, BIRBILIS N, SCULLY J R. A compilation of corrosion potentials for magnesium alloys [J]. Corrosion, 2014, 70(10): 1043−1051.
[29] KLOTZ D. Negative capacitance or inductive loop – A general assessment of a common low frequency impedance feature [J]. Electrochemistry Communications, 2019, 98: 58−62.
[30] DELGADO M C, GARCÍA-GALVAN F R, BARRANCO V, BATLLE S F. A measuring approach to assess the corrosion rate of magnesium alloys using electrochemical impedance spectroscopy [M]//Magnesium Alloys. 2017. https://doi.org/10. 5772/65018.
[31] KING A D, BIRBILIS N, SCULLY J R. Accurate electrochemical measurement of magnesium corrosion rates; a combined impedance, mass-loss and hydrogen collection study [J]. Electrochimica Acta, 2014, 121: 394−406.
[32] MENA-MORCILLO E, VELEVA L. Degradation of AZ31 and AZ91 magnesium alloys in different physiological media: Effect of surface layer stability on electrochemical behaviour [J]. Journal of Magnesium and Alloys, 2020, 8: 667−675.
[33] WU L, PAN F S, YANG M B, CHENG R J. An investigation of second phases in as-cast AZ31 magnesium alloys with different Sr contents [J]. Journal of Materials Science, 2013, 48: 5456−5469.
[34] CURIONI M. The behaviour of magnesium during free corrosion and potentiodynamic polarization investigated by real-time hydrogen measurement and optical imaging [J] Electrochimica Acta, 2014, 120: 284−292.
[35] CRITELLI R A J, BERTOTTI M, TORRESI R M. Probe effects on concentration profiles in the diffusion layer: Computational modeling and near-surface pH measurements using microelectrodes [J]. Electrochimica Acta, 2018, 292: 511−521.

氯离子浓度对 AZ63 镁合金初始腐蚀的影响

Branimir N. GRGUR[1], Branimir Z. JUGOVIĆ[2], Milica M. GVOZDENOVIĆ[1]

1. Faculty of Technology and Metallurgy, University of Belgrade, Karnegijeva 4, 11020 Belgrade, Serbia;
2. Serbian Academy of Science and Arts, Institute of Technical Science, Knez Mihailova 35, 11000 Belgrade, Serbia

摘　要：采用腐蚀电位、线极化、电化学阻抗谱和极化测量等方法研究 AZ63 镁合金在 1%、3%、5%和 7 % NaCl (质量分数)腐蚀介质中的初始腐蚀行为。结果表明，随着氯离子浓度的增加，腐蚀速率加快。基于得到的动力学参数，讨论了阳极溶解和析氢反应的机理，并建立了动力学模型。结果显示，阳极溶解是发生在 Temkin 条件下，析氢反应取决于 $Mg(OH)_2$ 的表面覆盖度。

关键词：氯化物；腐蚀电位；线极化；反应级数；动力学

(Edited by Xiang-qun LI)